High-efficiency photoelectrochemical hydrogen generation enabled by p-type semiconductor nanoparticle-decorated n-type nanotube arrays†

Lan Sun,[*a] Zhi Wu,[a] Siwan Xiang,[a] Jiangdong Yu,[a] Yingying Wang,[a] Changjian Lin[a] and Zhiqun Lin[*b]

TiO_2 nanotube arrays (TNTAs) were decorated with NiO nanoparticles *via* a sequential chemical bath deposition (CBD) approach to yield NiO@TNTA photoanodes. In sharp contrast to pure TNTAs, NiO@TNTAs displayed increased absorption and decreased photoluminescence. Interestingly, NiO@TNTA photoanodes exhibited a higher photoelectrochemical activity for hydrogen production than pure TNTAs. The incident-photon-to-current-conversion efficiency (IPCE) of the optimized NiO@TNTA photoanode was calculated to be 62.8%, and remarkably, the maximum hydrogen production rate reached 37.8 µmol h^{-1} cm^{-2}, approximately 5.0 times faster than pure TNTAs. Such markedly enhanced photoelectrochemical efficiency can be attributed primarily to the efficient separation of photogenerated charge carriers at the p–n junction of the two dissimilar semiconductors, that is, p-type NiO and n-type TiO_2, in conjunction with the implementation of nanosized NiO particles with large surface area which enables a shortened charge transfer distance and in turn increased probability of reaction of charge carriers with water molecules.

Introduction

Hydrogen generation *via* photocatalysis or photoelectrocatalysis using solar light has garnered much attention as it represents a potentially scalable means of storing solar energy in the form of clean and renewable hydrogen fuel.[1,2] Notably, solar hydrogen generation is accompanied by a largely positive change in Gibbs free energy, and thus it is an uphill reaction and a large amount of photogenerated electrons and holes tend to recombine during this process. Clearly, the effective charge separation and transport is of key importance in determining solar hydrogen generation efficiency.[3] As an n-type semiconductor, TiO_2 has been widely used as a photocatalyst in hydrogen generation.[4,5] When TiO_2 is irradiated by UV light, electrons and holes are generated. The photogenerated electrons reduce water to form hydrogen in a certain photocatalytic system while the photogenerated holes oxidize water to produce O_2. Owing to their large internal surface, excellent controllability and chemical stability, self-organized TiO_2 nanotube arrays (TNTAs) fabricated by electrochemical anodization of

high purity Ti foil have found a wide range of applications such as photoelectrolysis of water splitting,[6–8] dye-sensitized solar cells,[9,10] and photocatalytic degradation.[11] However, photocatalytic H_2 production efficiency using TiO_2 is limited due to high recombination rate of photogenerated electron–hole pairs. In addition, the utilization of solar energy by TiO_2 accounts for only approximately 3–5% of the entire solar spectrum due to its wide bandgap (*i.e.*, 3.2 eV for anatase and 3.0 eV for rutile). Thus, in recent years modifying TNTAs, for example, by deposition of noble metals,[12] dye sensitization,[13] metal cation doping,[14] carbon and nitrogen doping,[15,16] to yield improved photocatalytic activity has attracted considerable interest. Nevertheless, effective separation and transport of charge carriers to achieve efficient photocatalytic hydrogen production remains challenging.

Recently, constructing heterostructured photocatalysts have been extensively investigated and proven to be a particularly promising approach to improve photocatalytic hydrogen evolution efficiency.[1–3] Combining two different types of semiconductors with well-matched energy levels may facilitate the collection of photogenerated electrons and holes at the respective semiconductor surfaces, and thus enhance the separation of photogenerated charge carriers.[17] Over the past decades, a rich variety of semiconductor materials, including ZnO, Fe_2O_3, $BiVO_4$, CdS, C_3N_4 and Cu_2O, have been applied to form heterostructures with TiO_2.[18] Among various semiconductors, a p-type semiconductor NiO has received increasing attention due largely to its unique applications in

a State Key Laboratory of Physical Chemistry of Solid Surface, Department of Chemistry, College of Chemistry and Chemical Engineering, Xiamen University, Xianmen 361005, China. E-mail: sunlan@xmu.edu.cn

b School of Materials Science and Engineering, Georgia Institute of Technology, Atlanta, GA 30332, USA. E-mail: zhiqun.lin@mse.gatech.edu

† Electronic supplementary information (ESI) available. See DOI: 10.1039/c6ra27388b

many areas such as catalysis,[19] battery anode,[20] electrochemical super capacitors.[21,22] NiO has an indirect bandgap of approximately 3.55 eV, and its conduction band lies above that of TiO_2, which is energetically favorable and renders the photogenerated electrons to transfer from the conduction band of NiO to that of TiO_2. Notably, p–n junctions form at the interface when coupling n-type TiO_2 with p-type NiO. This induces an internal electric field that facilitates the separation of photogenerated electrons and holes.[23] Photocatalytic activity depends sensitively on the particle size and shape.[24] In a photocatalytic reaction there are three main processes: (i) absorption of photons to form electron–hole pairs; (ii) separation and migration of photogenerated carriers; and (iii) surface chemical reactions.[3] It is important to note that the faster the photogenerated charges transfer to surface to be involved in chemical reactions, the lower the probability of charge recombination is. Thus, the particle size plays an important role in the separation process of photogenerated charge carriers. For nanosized particles, a shorter distance is needed for photogenerated electrons and holes to migrate to the respective reaction sites on the surface, thereby leading to a decreased probability of electron–hole recombination.

Herein, we report highly efficient photoelectrocatalytic hydrogen generation achieved *via* a rational design of a p–n junction by impregnating nanosized NiO particles within well-ordered TiO_2 nanotube arrays (TNTAs). One-dimensional TNTAs composed of vertically oriented nanotubes were synthesized *via* three-step electrochemical anodization to reduce the structure disorders and defects. Subsequently, NiO nanoparticles with an average diameter of 7–10 nm were uniformly deposited within electrochemically anodized TNTAs through sequential chemical bath deposition. The resulting heterostructured NiO nanoparticles-decorated TNTAs (*i.e.*, NiO@TNTAs) were first employed for solar hydrogen production. Interestingly, under the optimized preparation condition for NiO@TNTAs, its hydrogen generation rate reached 37.8 $\mu mol\ h^{-1}\ cm^{-2}$, representing a 5-fold enhancement over that of pure TNTAs. Moreover, NiO@TNTAs exhibited an excellent stability over a period of 25 h. The enhanced photocatalytic H_2 evolution efficiency can be ascribed to the synergy of the promoted charge separation at the p–n junction composed of p-type NiO and n-type TiO_2 and the effective charge transport rendered by the implementation of NiO nanoparticles with large surface area.

Experimental section

Preparation of TiO_2 nanotube arrays (TNTAs)

Highly ordered TiO_2 nanotube arrays (TNTAs) with a regular porous surface topology were fabricated by a facile three-step electrochemical anodization of Ti foils (0.1 mm thick, 99.5% purity) according to our previous report.[25] An three-step electrochemical anodization was carried out in ethylene glycol solution containing 0.3 wt% NH_4F and 2 vol% H_2O at room temperature using Ti foil as a working electrode and platinum as a counter electrode, yielding highly ordered TiO_2 nanotubes. In the first-step anodization, Ti foil was anodized at 50 V for 5 h.

As-anodized Ti foil was then ultrasonically rinsed in acetone to strip the formed TiO_2 nanotubular layer from the Ti substrate. Subsequently, the second-step anodization of Ti substrate was performed at 50 V for 3 h to allow for the further growth of nanotubes and then ultrasonicated again to remove the resulting TiO_2 nanotubes. Finally, the third-step anodization was conducted on the exposed Ti foil at 50 V for 5 min, forming 1.2 µm-thick TiO_2 nanotube arrays situated on Ti foil. After rinsed with DI water and dried in air, as-prepared amorphous TiO_2 nanotube arrays were annealed to yield anatase crystalline phase at 350 °C for 2 h in air at the heating and cooling rates of 5 °C min^{-1}.

Synthesis of NiO@TNTAs

NiO nanoparticles were incorporated in TNTAs by sequence chemical bath deposition (CBD) technique. Briefly, 0.2 M $NiCl_2 \cdot 6H_2O$ ethanol solution and 0.2 M NH_4OH ethanol solution were prepared as precursor solutions. In a typical deposition cycle, TNTAs were immersed successively in $NiCl_2 \cdot 6H_2O$ ethanol solution for 2 min and then in NH_4OH ethanol solution for the same amount of time. Between each immersion step, samples were rinsed with ethanol adequately to remove the excess ions in TNTAs. Such immersion was repeated for several cycles (*i.e.*, 5, 10, 15 and 20). Upon the completion of deposition, samples were rinsed with DI water and dried in air. As-prepared samples were annealed in air at 550 °C for 1 h at heating rate of 5 °C min^{-1} to facilitate crystallization.

Characterizations and measurements

The morphology and structure of samples were characterized using field emission scanning electron microscope (FE-SEM, Hitachi S4800) and transmission electron microscopy (TEM, JEM 2100). The crystal phase and chemical composition of samples were identified by X-ray diffraction (XRD, Philips, Panalytical X'pert, Cu Kα radiation (λ = 1.5417 Å)) and X-ray photoelectron spectroscopy (XPS, VG, Physical Electrons Quantum 2000 Scanning ESCA Microprobe, Al Kα radiation), respectively. All XPS spectra were referenced to the C 1s peak at 284.8 eV from the adventitious carbon. UV-vis diffuse reflection spectroscopy (DRS) was recorded using a Varian Cary-5000 spectrophotometer. Photoluminescence (PL) spectra were obtained using fluorescence spectrophotometer (Hitachi F-7000) with xenon lamp as excitation source (λ = 370 nm) at room temperature.

Photocurrent measurements were performed in a three-electrode experimental system using a 263A potentiostat/galvanostat with an M5210 lock-in amplifier/chopper setup (using a chopper frequency of 34 Hz) connected to an SBP 300 grating spectrometer with an LHX 150 W Xe lamp as the source of illumination. As-prepared samples were used as a working electrode with a Pt foil as a counter electrode and a saturated calomel electrode (SCE) as a reference electrode in 0.5 M KOH electrolyte. The incident-photon-to-current-conversion efficiency, IPCE, at different wavelengths was determined from the short circuit photocurrent, I_{sc}, monitored at different excitation

wavelength, λ, to compare the photoresponse of samples using the following equation[26]

$$\text{IPCE} = \frac{1240 \times I_{sc}}{\lambda \times I_{inc}} \times 100$$

where I_{inc} is the incident light intensity.

The photoelectrocatalytic activity was investigated by monitoring the evolution of H_2 in the PEC cell containing 2 M Na_2CO_3 and 0.5 M ethylene glycol solution using a three-electrode system composed of the samples as a working electrode, a platinum sheet as a counter electrode, and a silver chloride electrode (Ag/AgCl) as a reference electrode, respectively. A LHX 300 Xe lamp (PLS-SXE300, Beijing Bofeilai Technology Co, Ltd) was employed as the simulate solar light source with a light intensity of 320 mW cm^{-2}.

Results and discussion

Highly ordered TNTAs were synthesized *via* a three-step electrochemical anodization of Ti foil. Subsequently, NiO nanoparticles were incorporated into the crystallized TiO_2 nanotubes by sequential chemical bath deposition (S-CBD) method, yielding NiO@TNTAs. The morphologies of TiO_2 nanotube films were examined using field-emission scanning electron microscope (FESEM). Fig. 1a and b show representative top and

Fig. 1 (a) Top and (b) cross-sectional views of SEM images of pure TiO_2 nanotube arrays (TNTAs). (c) Top and (d) cross-sectional views of FESEM images of NiO nanoparticles-decorated TNTAs. (e) TEM image of NiO nanoparticles-decorated TNTAs, and (f) the corresponding HRTEM image of NiO nanoparticles.

cross-sectional views of SEM images of as-synthesized TNTAs, respectively, after a three-step anodization (see Experimental section). Highly ordered tubular nanostructures are clearly evident. These vertically aligned nanotubes have an average inner tube diameter of 50 nm, tube wall thickness of 25 nm, and tube length of 1.2 μm. NiO nanoparticles were deposited into TNTAs *via* S-CBD for 5, 10, 15 and 20 cycles, respectively. The corresponding top-view SEM images are shown in Fig. S1.† Obviously, NiO nanoparticles were found to deposit effectively on the surface of TNTAs with a uniform size distribution as the immersion process of S-CBD increased from 5 to 15 cycles (Fig. S1a–c†). However, a further increase of immersion up to 20 cycles led to the agglomeration of NiO nanoparticles (Fig. S1d†). Importantly, well-ordered nanotubular structures retained, suggesting that the NiO nanoparticle deposition process did not alter the integrity of TNTAs. The best uniform dispersion of NiO nanoparticles with an average nanoparticle diameter of 7–10 nm was achieved from 15 cycles of CBD process. The top and cross-sectional views of FESEM images of NiO@TNTAs after 15-cycle immersions are displayed in Fig. 1c and d, respectively. It is clear that the surface of NiO@TNTAs is clean, and the diameter and wall thickness of the tube are approximately 50 nm and 25 nm, respectively (Fig. 1e), which is consistent with the SEM observation. NiO nanoparticles were homogeneously situated on the surface and the wall of TNTAs (Fig. 1e and f). The lattice spacing of 0.241 nm matches the inter-planar spacing of (101) crystallographic plane of NiO.

The elemental compositions of NiO@TNTAs were analyzed by X-ray photoelectron spectroscopy (XPS) (see Experimental section in ESI†). As shown in Fig. 2a, NiO@TNTAs samples contain Ti, O, Ni, and C elements. The carbon peak can be attributed to adventitious hydrocarbon from the XPS instrument. Fig. 2b depicts a high-resolution scan of XPS spectrum of Ni 2p region, which can be fitted into four peaks at 855.65 eV, 861.82 eV, 873.41 eV, and 879.63 eV. The binding energies of 855.65 eV and 861.82 eV correspond to Ni 2p$_{3/2}$, and the binding energies of 873.41 eV and 879.63 eV are attributed to Ni 2p$_{1/2}$, indicating the existence of NiO.[27,28] From the high-resolution XPS spectrum of O 1s shown in Fig. 2c, it can be seen that oxygen on the sample surface exists in the forms of metal oxide with the binding energies of 529.50 eV and 530.42 eV. The peak at 529.50 eV can be ascribed to O in TiO_2, and the peak at 530.42 eV is associated with O in NiO nanoparticles.[28,29] The XRD pattern of NiO@TNTAs clearly shows the diffraction of TiO_2 nanotubes and Ti foil with a diffraction peak of NiO (101) at $2\theta = 37.2°$ (ref. 30) (Fig. S2†). We note that the intensity of NiO peak was rather weak due to the limited amount of well-dispersed NiO nanoparticles on TNTAs.

Fig. S3† compares UV-vis diffuse reflectance spectra of NiO@TNTAs and pure TNTAs samples, respectively. Clearly, all NiO@TNTAs samples displayed red-shifts in absorbance and increased absorption intensity. The absorption edge of pure TNTAs at approximately 390 nm (*ca.* 3.2 eV) can be assigned to the intrinsic bandgap absorption of anatase TiO_2. It is interesting to note that the absorption range of NiO@TNTAs was gradually extended up to 550 nm as the immersion cycles of CBD process increased. Such an extension
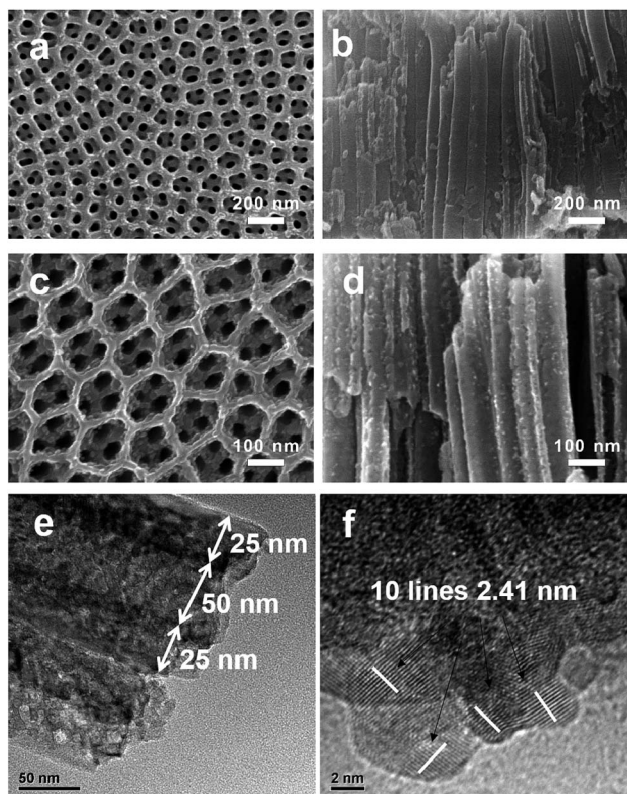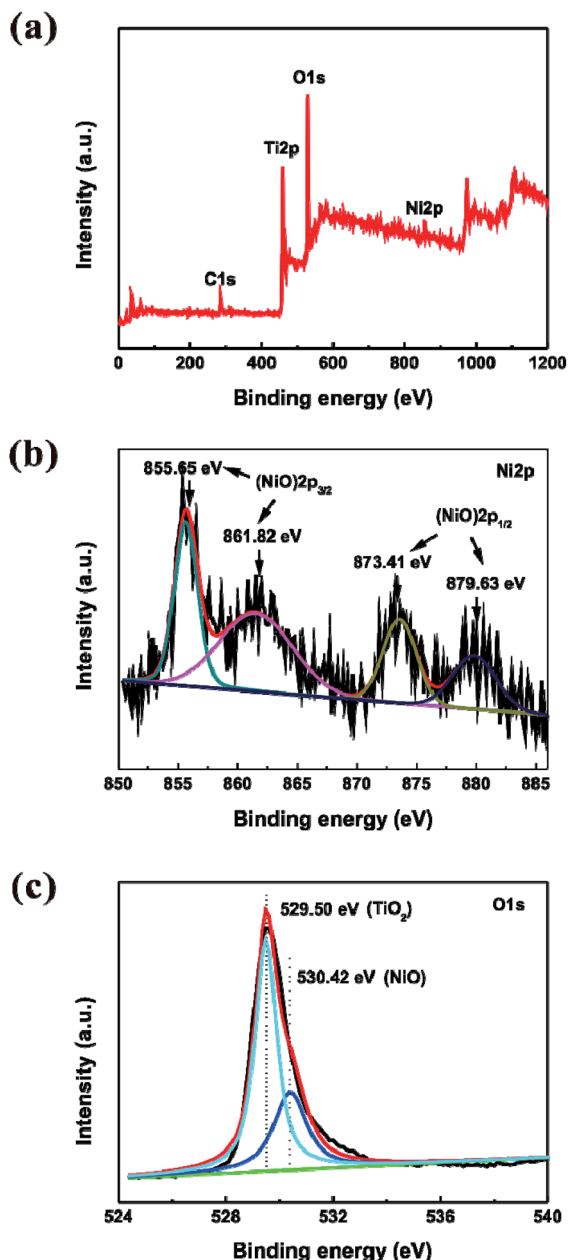
The separation of photogenerated electron–hole pairs was evaluated by measuring the photocurrent. Fig. 3 shows the current–voltage (*I–V*) and the current–time (*I–t*) characteristics of pure TNTAs and NiO@TNTAs. In Fig. 3a, the photocurrent of bare TNTAs electrodes was negligible. After the deposition of NiO nanoparticles, photocurrent density of NiO@TNTAs increased with increasing bias potential ranging from −0.8 V to 1.0 V as a result of the separation of the photogenerated electron–hole pairs. As shown in Fig. 3b, the photocurrent density of pure TNTAs was measured under 0.6 V bias *vs.* Ag/AgCl to be 0.35 mA cm^{-2} when irradiated. The photocurrent densities of the NiO@TNTAs prepared *via* 5, 10, 15 and 20 cycles of CBS were 0.43, 1.14, 2.04, 0.55 mA cm^{-2}, which was approximately 1.2,

Fig. 2 (a) XPS spectrum of NiO@TNTAs samples prepared by the CBD process for 15 cycles. (b–c) High-resolution XPS spectra of (b) Ni 2p and (c) O 1s, respectively.
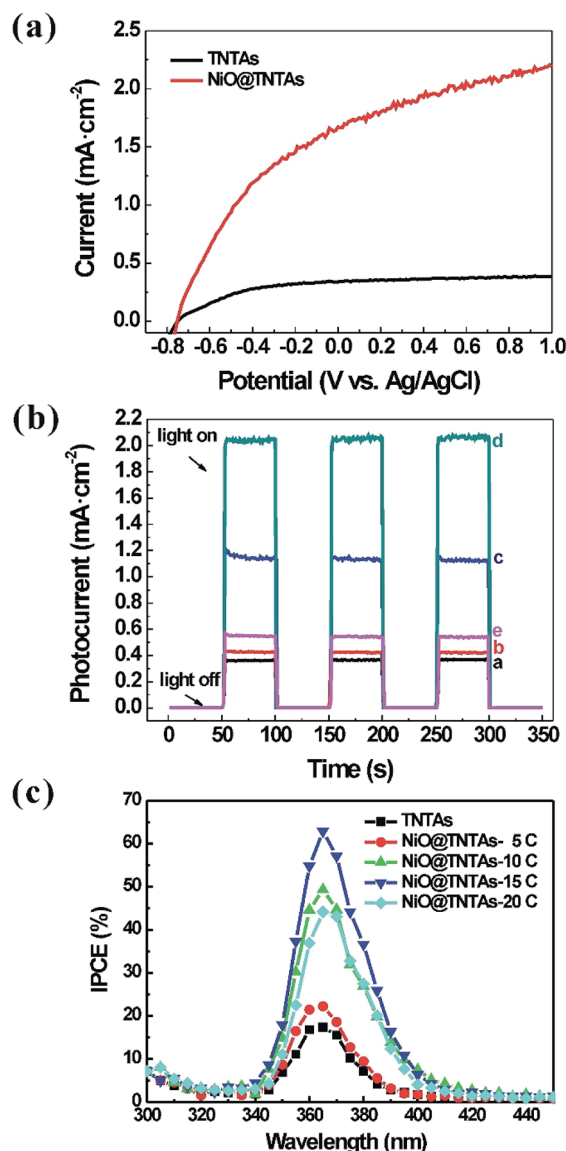

Fig. 3 Current–voltage characteristic (a) photocurrent response (b) and incident photon-to-current conversion efficiency (IPCE) (c) of pure TNTAs, NiO@TNTAs prepared *via* 5, 10, 15 and 20 cycles of CBS (denoted NiO@TNTAs-5C, NiO@TNTAs-10C, NiO@TNTAs-15C and NiO@TNTAs-20C, respectively) measured in 0.5 M KOH in a photoelectrochemical (PEC) cell.

may be owing to the reason that the overlap of Ti (d) orbit of TiO$_2$ and Ni (3d) orbit of NiO forms a new energy band in the TiO$_2$ bandgap, which decreases the energy gap between Ti (d) and O (p) orbitals in TiO$_2$, and in turn enables the adsorption of visible light.[31,32] The extension slightly decreased after the optimal 15-cycle deposition (*i.e.*, 20 cycles) due to the agglomeration of NiO nanoparticles. However, under visible light irradiation, the composite showed negligible photocurrent (Fig. S4†). No enhanced photocatalytic efficiency was observed in visible light region. This indicates that the red shift in the optical absorbance does not translate to the visible light photoelectrochemical activity.

3.3, 5.8, 1.6 times of that TNTAs, respectively. The enhanced photocurrent could be ascribed to the decoration of NiO into the TNTAs system, resulting in a higher separation efficiency of the photogenerated charges. Fig. 3c compares the incident photon-to-current conversion efficiency (IPCE) spectra. It is clear that NiO@TNTAs samples exhibited a significantly enhanced performance in comparison with pure TNTAs. A maximum IPCE of 62.8% at the wavelength of 365 nm was achieved for the NiO@TNTAs electrode prepared by S-CBD for 15 cycles, reflecting a nearly 3-fold increase compared to that of pure TNTAs (17.3%).

The interfacial properties between the electrode (*i.e.*, TNTAs and NiO@TNTAs) and the electrolyte were scrutinized by electrochemical impedance spectroscopy (EIS) measurements. Fig. 4 shows the Nyquist plots of the TNTAs and NiO@TNTAs under dark and light irradiation. The inset is the corresponding equivalent circuit and R_s, R_{ct} and CPE represent solution resistance, charge-transfer resistance and electronic double-layer capacitor, respectively. A semicircle in the Nyquist plot at high frequency represents the charge-transfer process, while the diameter of the semicircle reflects the R_{ct}. Clearly, the arches for NiO@TNTAs both in the dark and under irradiation were much smaller than those of TNTAs, implying that the decorated NiO nanoparticles on TNTAs significantly enhanced the electron mobility by inhibiting the recombination of electron–hole pairs.

It is well known that photoluminescence (PL) spectrum reflects the separation and recombination processes of photogenerated electron–hole pairs in semiconductor materials. To further verify the charge separation behavior and charge separation efficiency of NiO@TNTAs, PL spectra were measured (see Experimental section). In comparison with pure TNTAs, NiO@TNTAs exhibited a much lower PL intensity (Fig. 5). A low PL intensity signifies a long lifetime of photogenerated charge carriers with an enhanced separation of electrons trapped.[33] Thus, the largely quenched PL intensity suggested that NiO nanoparticles-decorated TNTAs greatly reduce the recombination rate of electron–hole pairs and consequently promoted the charge separation of photogenerated carriers, leading to a markedly enhanced photocatalytic activity.
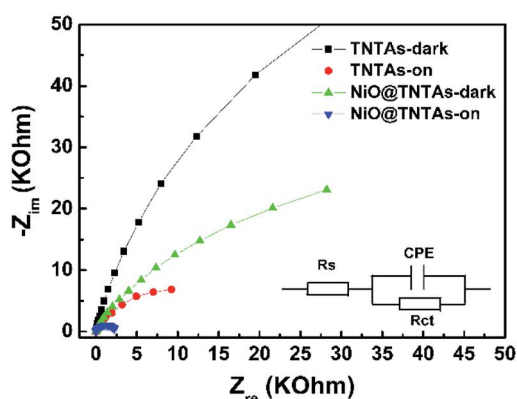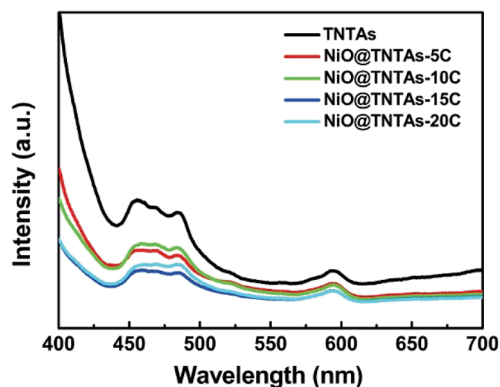

Fig. 5 PL spectra of TNTAs and NiO@TNTAs samples prepared after modified NiO nanoparticles by different cycles of CBD process.

To evaluate the photoelectrocatalytic activity of the NiO@TNTAs, the photoelectrochemical water splitting efficiency was then evaluated at a potential of 0.6 V *versus* Ag/AgCl in 2 M Na_2CO_3 and 0.5 M ethylene glycol in the PEC cell under Xe lamp (100 mW cm^{-2}) illumination (see Experimental section). Fig. 6a shows the hydrogen production rates of TNTAs
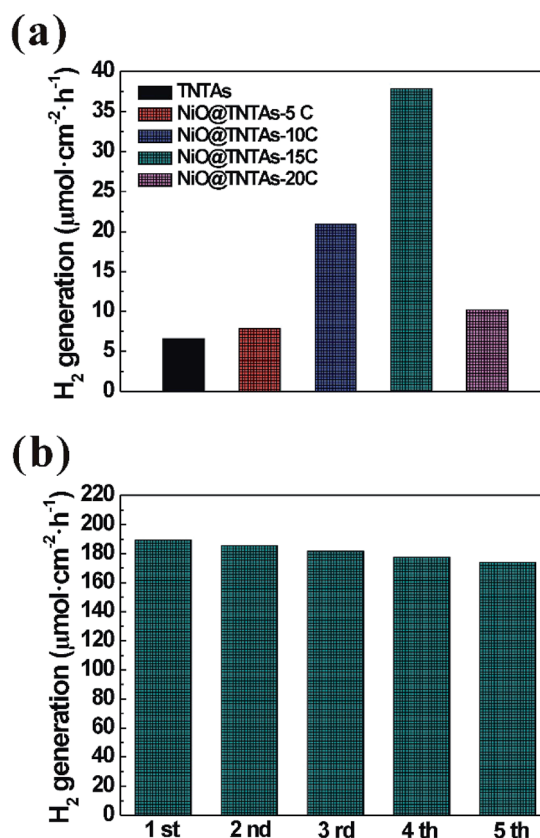

Fig. 6 (a) Hydrogen generation rate of TNTAs and NiO@TNTAs nanocomposites as photoanodes and Pt foil as cathodes at 0.6 V *vs.* Ag/AgCl with 2 M Na_2CO_3 and 0.5 M ethylene glycol solution in the PEC cell under Xe lamp (320 mW cm^{-2}) illumination. (b) Cycling hydrogen generation curve of the NiO@TNTAs electrode prepared by S-CBD for 15 cycles.

Fig. 4 Electrochemical impedance spectra of TNTAs and NiO@TNTAs in the dark and under Xe lamp irradiation.

and NiO@TNTAs prepared *via* 5, 10, 15 and 20 cycles of CBS. The pure TNTAs showed a very low evolution rate of hydrogen (6.5 μmol h^{-1} cm^{-2}) because of the rapid recombination between the conduction-band electrons and the valence-band holes. In sharp contrast, intriguingly, after the incorporation of NiO nanoparticles into pure TNTAs, in good correlation with the results of IPCE, the rate of hydrogen generation of NiO@TNTAs prepared by S-CBD for 15 cycles reached 37.8 μmol h^{-1} cm^{-2}, which is approximately 5.0 times faster than that of pure TNTAs. With a further increase of the immersion cycles, the rate of hydrogen generation of NiO@TNTAs decreased to 10.2 μmol h^{-1} cm^{-2}. This is not surprising because NiO nanoparticles aggregated and restricted the transfer of photogenerated charge carriers, as noted above. It is noteworthy that the NiO@TNTAs electrode was remarkably stable and did not deteriorate with time (Fig. 6b). Even the fifth cycle was performed, no reduction in the rate of hydrogen production was observed.

The enhanced photoelectrochemical efficiency and photocatalytic activity of hydrogen production can be attributed primarily to the p–n junction effect formed by decorating p-type NiO on n-type TiO$_2$ nanotube surface. A schematic diagram of energy band structure and electron–hole pair separation at the p–n junction composed of p-type NiO and n-type TiO$_2$ is illustrated in Fig. 7. The Fermi energy levels of n-type TiO$_2$ lies closer to its conduction band, and the Fermi energy level of p-type NiO situates near to its valence band.[23] When placing these two types of semiconductors in contact, the electron transfers from TiO$_2$ to NiO, and the hole transfers from NiO to TiO$_2$ due to the carrier diffusion between NiO and TiO$_2$ until the thermal equilibration is reached, forming a constant Fermi energy.[23,34] Such carrier diffusion process makes p-type semiconductor NiO region negatively charged, while TiO$_2$ region has the positive charge. Thus, an inner electric field is built-up at the interface.[35] Under illumination, the photogenerated electron–hole pairs transfer in the opposite direction driven by the inner electric field, *i.e.*, the photogenerated holes at the valence band of TiO$_2$ flow into NiO and then were consumed by the sacrificial reagent, while the photogenerated electrons on NiO move to TiO$_2$ and then transfer to the Pt counter electrode, where H$_2$ evolution

takes place.[23] Consequently, the photogenerated electron–hole pairs are efficiently separated, resulting in enhanced photocatalytic activity, as corroborated by the PL measurements (Fig. 5). In addition, the implementation of NiO nanoparticles possessing high specific surface area is advantageous as they offer the increased active sites and shortened pathway for photogenerated charge carriers to migrate to the surface of electrode, which raise the probability of reaction of photogenerated electrons and holes with water molecules, and thus increase photocatalytic H$_2$ generation rate. Meanwhile, NiO nanoparticles can also act as holes traps and collectors, promoting the separation of photogenerated charge carriers.[36,37]

Conclusions

In summary, highly ordered one-dimensional NiO@TNTAs heterostructures comprising well-dispersed p-type NiO nanoparticles decorated on electrochemically anodized n-type TiO$_2$ nanotube arrays were crafted by simple yet effective sequential chemical bath deposition technique. Heterostructured NiO@TNTAs was then exploited as an active and stable electrode for hydrogen generation. The optimized NiO@TNTAs displayed an IPCE of 62.8% at 365 nm, which is nearly 3 times higher than that of pure TNTAs. Moreover, an impressive hydrogen production rate of 37.8 μmol h^{-1} cm^{-2} was achieved, representing approximately 5-fold enhancement over pure TNTAs. This highly efficient photoelectrocatalytic hydrogen generation may be a direct consequence of effective separation of photogenerated charge carriers enabled by the formation of p–n junction between p-type NiO and n-type TiO$_2$, and the use of nanosized NiO particles that render a shortened charge transfer distance and thus an increased probability of reaction of charges with water molecules. Clearly, crafting of p–n junction may stand out as a simple yet robust route to the improved solar energy conversion involving TiO$_2$ by effectively addressing the limiting factors described above.

Acknowledgements

References

1 T. Hisatomi, J. Kubota and K. Domen, Recent advances in semiconductors for photocatalytic and photoelectrochemical water splitting, *Chem. Soc. Rev.*, 2014, **43**, 7520–7535.

2 H. Li, Y. Zhou, W. Tu, J. Ye and Z. Zou, State-of-the-Art Progress in Diverse Heterostructured Photocatalysts toward Promoting Photocatalytic Performance, *Adv. Funct. Mater.*, 2015, **25**, 998–1013.

3 A. Kudo and Y. Miseki, Heterogeneous photocatalyst materials for water splitting, *Chem. Soc. Rev.*, 2009, **38**, 253–278.
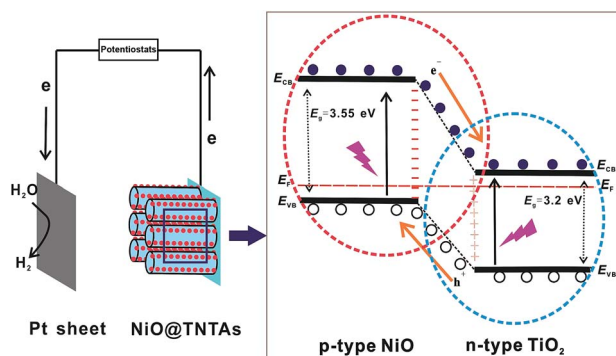

Fig. 7 Schematic illustration of charge transfer process between p-type NiO and n-type TiO$_2$.

4 D. Y. Leung, X. Fu, C. Wang, M. Ni, M. K. Leung, X. Wang and X. Fu, Hydrogen production over titania-based photocatalysts, *ChemSusChem*, 2010, **3**, 681–694.

5 R. Marschall, Semiconductor Composites: Strategies for Enhancing Charge Carrier Separation to Improve Photocatalytic Activity, *Adv. Funct. Mater.*, 2014, **24**, 2421–2440.

6 S. K. Mohapatra, M. Misra, V. K. Mahajan and K. S. Raja, A novel method for the synthesis of titania nanotubes using sonoelectrochemical method and its application for photoelectrochemical splitting of water, *J. Catal.*, 2007, **246**, 362–369.

7 J. Yu, C. Gong, Z. Wu, Y. Wu, W. Xiao, Y. Su, L. Sun and C. Lin, Efficient visible light-induced photoelectrocatalytic hydrogen production using CdS sensitized TiO₂ nanorods on TiO₂ nanotube arrays, *J. Mater. Chem. A*, 2015, **3**, 22218–22226.

8 I. S. Cho, J. Choi, K. Zhang, S. J. Kim, M. J. Jeong, L. Cai, T. Park, X. Zheng and J. H. Park, Highly Efficient Solar Water Splitting from Transferred TiO₂ Nanotube Arrays, *Nano Lett.*, 2015, **15**, 5709–5715.

9 J. Wang and Z. Lin, Dye-Sensitized TiO₂ Nanotube Solar Cells with Markedly Enhanced Performance *via* Rational Surface Engineering, *Chem. Mater.*, 2010, **22**, 579–584.

10 M. Ye, D. Zheng, M. Lv, C. Chen, C. Lin and Z. Lin, Hierarchically structured nanotubes for highly efficient dye-sensitized solar cells, *Adv. Mater.*, 2013, **25**, 3039–3044.

11 M. Wang, J. Ioccozia, L. Sun, C. Lin and Z. Lin, Inorganic-modified semiconductor TiO₂ nanotube arrays for photocatalysis, *Energy Environ. Sci.*, 2014, **7**, 2182.

12 M. Ye, J. Gong, Y. Lai, C. Lin and Z. Lin, High-efficiency photoelectrocatalytic hydrogen generation enabled by palladium quantum dots-sensitized TiO₂ nanotube arrays, *J. Am. Chem. Soc.*, 2012, **134**, 15720–15723.

13 M. Myahkostupov, M. Zamkov and F. N. Castellano, Dye-sensitized photovoltaic properties of hydrothermally prepared TiO₂ nanotubes, *Energy Environ. Sci.*, 2011, **4**, 998–1010.

14 A. El Ruby Mohamed and S. Rohani, Modified TiO₂ nanotube arrays (TNTAs): progressive strategies towards visible light responsive photoanode, a review, *Energy Environ. Sci.*, 2011, **4**, 1065–1086.

15 R. Asahi, T. Morikawa, T. Ohwaki, K. Aoki and Y. Taga, Visible-Light Photocatalysis in Nitrogen-Doped Titanium Oxides, *Science*, 2001, **293**, 269–271.

16 S. U. M. Khan, M. Al-Shahry and W. B. Ingler, Efficient Photochemical Water Splitting by a Chemically Modified n-TiO₂, *Science*, 2002, **297**, 2243–2245.

17 S. J. A. Moniz, J. Zhu and J. Tang, 1D Co-Pi Modified BiVO₄/ZnO Junction Cascade for Efficient Photoelectrochemical Water Cleavage, *Adv. Energy Mater.*, 2014, **4**, 1301590–1301597.

18 S. J. Moniz, S. A. Shevlin, D. J. Martin, Z.-X. Guo and J. Tang, Visible-light driven heterojunction photocatalysts for water splitting–a critical review, *Energy Environ. Sci.*, 2015, **8**, 731–759.

19 J. Park, E. Kang, S. U. Son, H. M. Park, M. K. Lee, J. Kim, K. W. Kim, H. J. Noh, J. H. Park, C. J. Bae, J. G. Park and T. Hyeon, Monodisperse Nanoparticles of Ni and NiO: Synthesis, Characterization, Self-Assembled Superlattices, and Catalytic Applications in the Suzuki Coupling Reaction, *Adv. Mater.*, 2005, **17**, 429–434.

20 H. Liu, G. Wang, J. Liu, S. Qiao and H. Ahn, Highly ordered mesoporous NiO anode material for lithium ion batteries with an excellent electrochemical performance, *J. Mater. Chem.*, 2011, **21**, 3046–3052.

21 J.-W. Lang, L.-B. Kong, W.-J. Wu, Y.-C. Luo and L. Kang, Facile approach to prepare loose-packed NiO nano-flakes materials for supercapacitors, *Chem. Commun.*, 2008, 4213–4215, DOI: 10.1039/b800264a.

22 C. Yuan, X. Zhang, L. Su, B. Gao and L. Shen, Facile synthesis and self-assembly of hierarchical porous NiO nano/micro spherical superstructures for high performance supercapacitors, *J. Mater. Chem.*, 2009, **19**, 5772–5777.

23 J. Yu, W. Wang and B. Cheng, Synthesis and Enhanced Photocatalytic Activity of a Hierarchical Porous Flowerlike p–n Junction NiO/TiO₂ Photocatalyst, *Chem.–Asian J.*, 2010, **5**, 2499–2506.

24 Y.-F. Li and Z.-P. Liu, Particle size, shape and activity for photocatalysis on titania anatase nanoparticles in aqueous surroundings, *J. Am. Chem. Soc.*, 2011, **133**, 15743–15752.

25 J. Gong, Y. Lai and C. Lin, Electrochemically multi-anodized TiO₂ nanotube arrays for enhancing hydrogen generation by photoelectrocatalytic water splitting, *Electrochim. Acta*, 2010, **55**, 4776–4782.

26 I. Robel, V. Subramanian, M. Kuno and P. V. Kamat, Quantum Dot Solar Cells, Harvesting Light Energy with CdSe Nanocrystals Molecularly Linked to Mesoscopic TiO₂ Films, *J. Am. Chem. Soc.*, 2006, **128**, 2385–2393.

27 V. Biju, Ni 2p X-ray photoelectron spectroscopy study of nanostructured nickel oxide, *Mater. Res. Bull.*, 2007, **42**, 791–796.

28 B. Sasi and K. Gopchandran, Nanostructured mesoporous nickel oxide thin films, *Nanotechnology*, 2007, **18**, 115613–115621.

29 L. C. Sim, K. W. Ng, S. Ibrahim and P. Saravanan, Preparation of Improved p–n Junction NiO/TiO₂ Nanotubes for Solar-Energy-Driven Light Photocatalysis, *Int. J. Photoenergy*, 2013, **2013**, 1–10.

30 K. Arshak, O. Korostynska and F. Fahim, *Various Structures Based on Nickel Oxide Thick Films as Gamma Radiation Sensors*, 2003, vol. 3, pp. 176–186.

31 J. Guo, W. Fu, H. Yang, Q. Yu, W. Zhao, X. Zhou, Y. Sui, J. Ding, Y. Li, S. Cheng and M. Li, A NiO/TiO₂ junction electrode constructed using self-organized TiO₂ nanotube arrays for highly efficient photoelectrocatalytic visible light activations, *J. Phys. D: Appl. Phys.*, 2010, **43**, 245202.

32 G. K. Mor, H. E. Prakasam, O. K. Varghese, K. Shankar and C. A. Grimes, Vertically oriented Ti–Fe–O nanotube array films: toward a useful material architecture for solar spectrum water photoelectrolysis, *Nano Lett.*, 2007, **7**, 2356–2364.

33 K. Xie, Q. Wu, Y. Wang, W. Guo, M. Wang, L. Sun and C. Lin, Electrochemical construction of Z-scheme type CdS–Ag–TiO$_2$ nanotube arrays with enhanced photocatalytic activity, *Electrochem. Commun.*, 2011, **13**, 1469–1472.

34 Z. Zhang, C. Shao, X. Li, C. Wang, M. Zhang and Y. Liu, Electrospun nanofibers of p-type NiO/n-type ZnO heterojunctions with enhanced photocatalytic activity, *ACS Appl. Mater. Interfaces*, 2010, **2**, 2915–2923.

35 C. Shifu, Z. Sujuan, L. Wei and Z. Wei, Preparation and activity evaluation of p–n junction photocatalyst NiO/TiO$_2$, *J. Hazard. Mater.*, 2008, **155**, 320–326.

36 C.-C. Hu and H. Teng, Structural features of p-type semiconducting NiO as a co-catalyst for photocatalytic water splitting, *J. Catal.*, 2010, **272**, 1–8.

37 N. K. Shrestha, M. Yang, Y.-C. Nah, I. Paramasivam and P. Schmuki, Self-organized TiO$_2$ nanotubes: Visible light activation by Ni oxide nanoparticle decoration, *Electrochem. Commun.*, 2010, **12**, 254–257.